Letter

Spinon continuum in the Heisenberg quantum chain compound $Sr_2V_3O_9$

Shang Gao,[1,2,3,*] Ling-Fang Lin,[4] Pontus Laurell,[4] Qiang Chen,[4] Qing Huang,[4] Clarina dela Cruz,[1] Krishnamurthy V. Vemuru,[1,5] Mark D. Lumsden,[1] Stephen E. Nagler,[1,4] Gonzalo Alvarez,[6] Elbio Dagotto,[2,4] Haidong Zhou,[4] Andrew D. Christianson,[2] and Matthew B. Stone[1,†]

[1]*Neutron Scattering Division, Oak Ridge National Laboratory, Oak Ridge, Tennessee 37831, USA*
[2]*Materials Science & Technology Division, Oak Ridge National Laboratory, Oak Ridge, Tennessee 37831, USA*
[3]*Department of Physics, University of Science and Technology of China, Hefei, Anhui 230026, People's Republic of China*
[4]*Department of Physics and Astronomy, University of Tennessee, Knoxville, Tennessee 37996, USA*
[5]*BrainChip Inc., Laguna Hills, California 92653, USA*
[6]*Computational Sciences & Engineering Division, Oak Ridge National Laboratory, Oak Ridge, Tennessee 37831, USA*

(Received 22 July 2023; revised 4 November 2023; accepted 13 December 2023; published 4 January 2024)

Magnetic excitations in the spin chain candidate $Sr_2V_3O_9$ have been investigated by inelastic neutron scattering on a single crystal sample. A spinon continuum with a bandwidth of ∼22 meV is observed along the chain formed by alternating magnetic V^{4+} and nonmagnetic V^{5+} ions, which reveals the importance of the orbital degree of freedom in determining the chain axis as identified by prior electronic structure calculations. Incipient magnetic Bragg peaks due to weak ferromagnetic interchain couplings emerge when approaching the magnetic transition at $T_N \sim 5.3$ K, while the excitations remain gapless within the instrumental resolution. Comparisons to the Bethe ansatz, density matrix renormalization group calculations, and effective field theories confirm $Sr_2V_3O_9$ as a host of weakly coupled $S = 1/2$ chains dominated by antiferromagnetic intrachain interactions of ∼7.1(1) meV.

DOI: 10.1103/PhysRevB.109.L020402

Introduction. Spin chains are one of the simplest models that illustrate many fundamental concepts in quantum magnets [1]. The reduced number of neighboring sites greatly enhances quantum fluctuations and promotes exotic phenomena like spinon excitations [2,3] and valence bonds [4]. Compared to higher dimensional systems, an advantage of the chain models is that they can be solved with high accuracy [5]. Starting from the Bethe ansatz for the $S = 1/2$ Heisenberg chains [2], analytical or numerical solutions for spin chains have been obtained for various types of chains that incorporate perturbations like Ising anisotropy, interchain couplings, and magnetic fields, thus allowing a thorough understanding of a plethora of novel phenomena including Zeeman ladders [6–10], psinon excitations [11,12], and Bethe strings [13–18].

The strontium vanadate $Sr_2V_3O_9$ has been proposed as a host of the $S = 1/2$ Heisenberg antiferromagnetic chain (HAFMC) [19,20]. $Sr_2V_3O_9$ belongs to the monoclinic $C2/c$ space group, with lattice constants determined as $a = 7.55$, $b = 16.28$, $c = 6.95$ Å, and $\beta = 119.78°$ [21]. We note that Refs. [19,20] use a different crystal structure than we use where the $\boldsymbol{c}$ axis corresponds to our $\boldsymbol{a} + \boldsymbol{c}$ axis. In $Sr_2V_3O_9$, the V-O layers in the ac planes are separated at a large distance of ∼8.14 Å by the Sr layers along the $\boldsymbol{b}$ axis. As shown in the inset of Fig. 1, within the V-O layers, the $V^{4+}O_6$ octahedra containing the magnetic V^{4+} ions ($S = 1/2$) share corners along the $\boldsymbol{a} + \boldsymbol{c}$ direction, denoted as [101] in real space. The V^{4+} ions inside the octahedra are displaced towards the shared apical oxygen ions. Along the $\boldsymbol{a} - \boldsymbol{c}$ direction, denoted as $[10\bar{1}]$, the $V^{4+}O_6$ octahedra are linked across the nonmagnetic $V^{5+}O_4$ tetrahedra. Surprisingly, thermal transport measurements on a crystal sample indicate the spin chains are along the $[10\bar{1}]$ direction [22,23], suggesting stronger spin couplings across the nonmagnetic $V^{5+}O_4$ tetrahedra. Although such a scenario was first proposed by both extended Hückel tight binding (EHTB) electronic structure calculations [24] and density functional theory (DFT) calculations [25,26], direct spectroscopic evidence for chain physics in $Sr_2V_3O_9$ is still missing.

Here we utilize neutron scattering to study the spin dynamics in $Sr_2V_3O_9$. A gapless spinon continuum, which is a characteristic feature of the $S = 1/2$ Heisenberg chain, is observed at temperatures down to ∼5 K. The chain direction is determined to be along the $\boldsymbol{a} - \boldsymbol{c}$ direction, thus verifying the scenario deduced from the thermal transport experiments [22,23] and confirming the importance of the orbital degree of freedom in determining the chain axis [24–26]. By comparing inelastic neutron scattering (INS) spectra with the Bethe ansatz, density matrix renormalization group (DMRG) calculations, and field theories, we conclude that $Sr_2V_3O_9$ hosts weakly coupled $S = 1/2$ HAFMCs.

Methods. $Sr_2V_3O_9$ crystals were prepared using a floating zone image furnace following reported procedures [22]. In order to synthesize phase pure $Sr_2V_3O_9$, polycrystalline $Sr_2V_2O_7$ was first prepared using a stoichiometric $SrCO_3$ and V_2O_5 powder mixture fired at 700 °C for 72 h in air. The obtained $Sr_2V_2O_7$ powder was then mixed with VO_2

*sgao.physics@gmail.com
†stonemb@ornl.gov

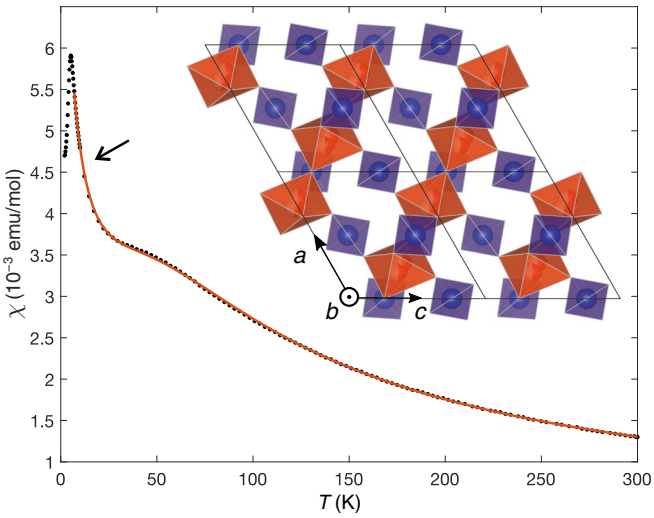

FIG. 1. Magnetic susceptibility of $Sr_2V_3O_9$ measured in a 5 kOe field. An antiferromagnetic transition is observed at $T_N = 5.3$ K as a sharp peak. The black arrow indicates the upturn in $\chi(T)$ above T_N. The red solid line is the fit to the $\chi(T)$ in the temperature range of [10, 300] K, as described in the text. The inset is the $Sr_2V_3O_9$ crystallographic structure viewed along the $\boldsymbol{b}$ axis. The $V^{4+}O_6$ octahedra and $V^{5+}O_4$ tetrahedra are shown in red and blue, respectively. V^{4+} ions inside the $V^{4+}O_6$ octahedra are displaced towards one of the two apical oxygen atoms shared by the neighboring $V^{4+}O_6$ octahedra. The positions of the Sr^{2+} ions are not shown for clarity.

powder in a molar ratio of 1:1. The mixture was pressed into a rod of ∼7 mm in diameter, ∼10 cm in length, and then annealed at 540 °C in argon for 24 h. The following floating zone growth was performed using a NEC two-mirror image furnace. As is reported in Ref. [22], the twice-scanning technique is utilized for this growth. The first scan was a fast scan with a speed of 35 mm/h under flowing Ar of 2.5 atm. The second growth scan was done using a speed of 1 mm/h in the same gas flow. Several large segments of single crystal were obtained. These crystals were then oriented by backscattering x-ray Laue diffraction in preparation for the neutron scattering measurements. dc magnetic susceptibility measurements were performed at temperatures of 2–300 K using a Quantum Design superconducting quantum interference device–vibrating sample magnetometer (SQUID-VSM). The sample was cooled in zero field (ZFC) and measured in an external field of 0.5 T for increasing temperatures.

Inelastic neutron scattering (INS) experiments on $Sr_2V_3O_9$ were performed on the fine-resolution Fermi chopper spectrometer SEQUOIA at the Spallation Neutron Source (SNS) of the Oak Ridge National Laboratory (ORNL). A single crystal with mass of ∼200 mg was aligned with the $\boldsymbol{b}$ axis vertical. A closed cycle refrigerator (CCR) was employed to reach temperatures, T, down to 5 K. Incident neutron energies were $E_i = 35$, 10, and 4 meV. For the $E_i = 35$ meV measurements, a Fermi chopper frequency of 240 Hz was used with the high flux chopper. Data were acquired by rotating the sample in 1° steps about its vertical axis, covering a total range of 165° at $T = 5$, 20, and 50 K. For the $E_i = 10$ and 4 meV measurements, a Fermi chopper frequency of 120 Hz was used with the high resolution chopper. Data for the $E_i = 10$ meV (4 meV) measurements at 4 K were acquired by rotating the sample in 1° (0.4°) steps, covering a total range of 200° (39.2°). Measurements of an empty sample holder were subtracted as the background. Data reductions and projections were performed using the MANTID software [27].

For the theoretical calculations, the canonical one-dimensional isotropic $S = 1/2$ HAFMC model described by the Hamiltonian $\mathcal{H} = J\sum_{\langle NN\rangle} \mathbf{S}_i \cdot \mathbf{S}_j$ is adopted, where the summation is over the nearest neighbors (NN) along the chain direction. The $T = 0$ dynamical spin structure factor was calculated in the algebraic Bethe ansatz approach using the ABACUS algorithm [28]. The calculation was performed on a system of $L = 500$ sites with periodic boundary conditions, using an energy step of $\Delta\omega = 0.002J$. A Gaussian energy broadening of $0.02J \approx 0.142$ meV was applied. A sum rule saturation of 99% was reached, which can be compared with the approximately 98% saturation expected from the two- and four-spinon contributions to the total intensity in the thermodynamic limit [29].

Theoretical spectra were also calculated using the density matrix renormalization group (DMRG) technique [30,31] as implemented in the DMRG++ code [32]. The calculations were carried out using the Krylov-space correction vector approach [33,34] with open boundary conditions. Targeting a truncation error below 10^{-10}, a minimum of 100 and up to 1000 states were kept during our DMRG calculations. The half width at half maximum of the Lorentzian energy broadening was set as $0.1J$. For the $T = 0$ DMRG calculations, we used a chain with $N = 100$ sites, while for the $T > 0$ calculations we adopted a system of 50 physical and 50 ancilla sites, using the ancilla (or purification) method [35–37]. Examples of input files and more details can be found in the Supplemental Material [38].

Results and discussions. As a reference for the temperature evolution of the spin correlations, Fig. 1 presents the magnetic susceptibility $\chi(T)$ measured on pulverized single crystals of $Sr_2V_3O_9$. A broad hump around $T = 50$ K signals strong short-range spin correlations. Following Ref. [19], we fit $\chi(T)$ to $\chi_{1D} + \chi_{LT} + \chi_{vv}$, where χ_{1D} is the polynomial approximation of the contribution from a $S = 1/2$ Heisenberg chain [40], χ_{LT} is a Curie-Weiss term to account for the upturn at low temperatures, and χ_{vv} is a temperature-independent Van Vleck contribution. The fitted intrachain coupling strength is $J = 6.95(5)$ meV, which is close to the previously reported value [19]. An antiferromagnetic transition is observed at $T_N \sim 5.3$ K, indicating the existence of weak interchain couplings $J_\perp$. An upturn in $\chi(T)$ starting at ∼25 K down to T_N, which is described by the χ_{LT} term, has been ascribed to the antisymmetric Dyaloshinskii-Moriya (DM) interactions [19,20], although such a scenario cannot be directly verified in our zero-field experiments [41,42].

The existence of a magnetic ordered state below T_N is directly confirmed by the neutron scattering data measured at $T = 5$ K. For the elastic map shown in the left panel of Fig. 2(a), the data collected at $T = 50$ K is subtracted to expose the weak magnetic reflections. Unless otherwise stated, all presented neutron scattering data are integrated along the $(0,k,0)$ direction in the range of $k = [-4, 4]$ reciprocal lattice units (r.l.u.) to improve counting statistics. Therefore, the strongest magnetic reflection in Fig. 2(a), $(1/2, k, -1/2)$,

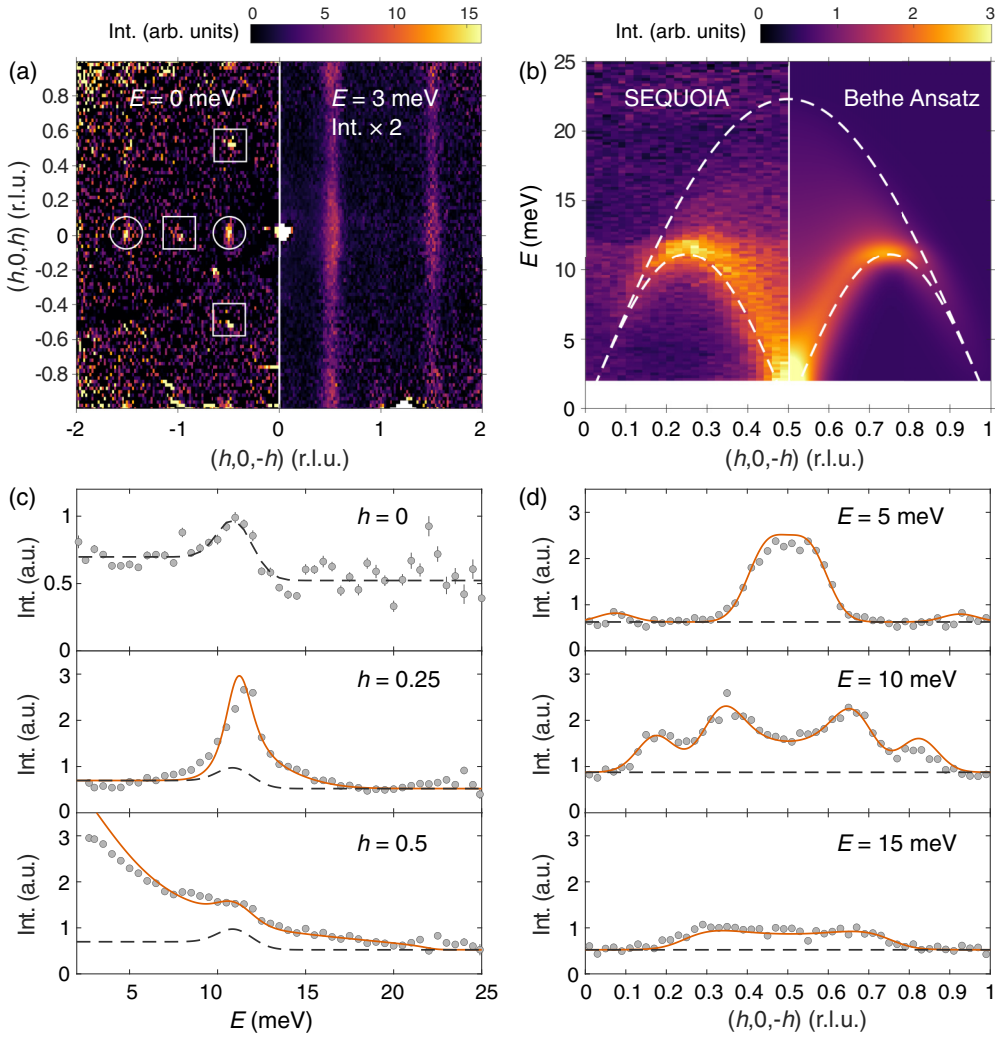

FIG. 2. (a) Constant energy slices of the $Sr_2V_3O_9$ INS spectra $S(Q, \omega)$ in the $(h, 0, l)$ plane at $E = 0$ and 3 meV integrated over the energy range of $[-2, 2]$ and [2,4] meV, respectively. Data is plotted on an orthogonal coordinate system for clarity. The incident neutron energy is $E_i = 35$ meV with the measuring temperature $T = 5$ K. Intensity in the slice at $E = 3$ meV is multiplied by a factor of 2 for better visibility. In the $E = 0$ meV slice, circles and squares indicate the magnetic and nuclear Bragg peaks, respectively. (b) Comparison between the experimental and theoretical $S(Q, \omega)$ along the $(h, 0, \bar{h})$ direction. The experimental data is integrated over the range of $\delta h = [-1.2, 1.2]$ r.l.u. along $(h, 0, h)$. For the calculated cross section, a constant intensity is added to account for any measurement background. Dashed lines are the lower and upper boundaries of the 2-spinon continuum for $J = 7.1$ meV. (c) Scattering intensity as a function of E at $h = 0$, 0.25, and 0.5 along $(h, 0, \bar{h})$. The black dashed line is a fit to the background scattering at $h = 0$ using a Gaussian function plus a step function. The red solid line is a fit to the spinon continuum plus the background. (d) Scattering intensity as a function of $(h, 0, \bar{h})$ at $E = 5$, 10, and 15 meV. The black dashed line indicates the constant background extracted from the scan at $h = 0$ in panel (c). The red solid line is a fit to the spinon continuum plus the background. The abbreviation a.u. for intensity stands for arbitrary units.

can be indexed as $(1/2, 1, -1/2)$, revealing the magnetic propagation vector to be $\boldsymbol{q} = (1/2, 0, 1/2)$. As this $\boldsymbol{q}$ vector indicates parallel spin alignment along the $\boldsymbol{a} + \boldsymbol{c}$ direction, we can conclude that the weak interchain coupling should be ferromagnetic assuming a collinear spin alignment along the chain with the strongest interchain couplings arising from the corner-sharing $V^{4+}O_6$ octahedra along the $\boldsymbol{a} + \boldsymbol{c}$ direction. Previous DFT calculations also reveal such interchain couplings to be ferromagnetic [25]. A thorough examination of the magnetic structure will be useful to fully confirm the assumption of a collinear magnetic order.

At an energy transfer of $E = 3$ meV, the constant energy map shown in the right panel of Fig. 2(a) exhibits narrow streaks along the $(h, 0, h)$ direction. Such a highly anisotropic scattering pattern is direct evidence for the emergence of spin chains in $Sr_2V_3O_9$, with chains running along the $\boldsymbol{a} - \boldsymbol{c}$ direction. Considering that the displacement of the V^{4+} ions inside the octahedra relieves the degeneracy of the t_{2g} orbitals [19,20], leaving the d_{xy} orbital as the ground state configuration and thus greatly reducing the orbital overlapping along the V^{4+}-O^{2-}-V^{4+} exchange path along the $\boldsymbol{a} + \boldsymbol{c}$ direction, the observation of spin chains along the $\boldsymbol{a} - \boldsymbol{c}$ direction directly confirms the importance of the orbital degree of freedom in determining the chain axis [24–26]. Weak modulation along the streaks can be ascribed to the perturbations due to interchain couplings. In the Supplemental Material

[38], we present slices along the $(0, k, 0)$ and $(h, 0, h)$ directions, which reveal very weakly dispersive excitations due to marginal interchain couplings.

After integrating the INS data along the $(h, 0, h)$ direction within a range of $\delta h = [-1.2, 1.2]$ r.l.u., the excitation spectra along the $(h, 0, \bar{h})$ direction are obtained. As shown in the left panel of Fig. 2(b), the spectra exhibit a continuum of excitations up to ∼22 meV, which is a typical feature of fractional spinon excitations of HAFMCs [43–47]. The lower and upper boundaries of the 2-spinon continuum can be described by $\omega_L(q) = (\pi/2)J|\sin q|$ and $\omega_U(q) = \pi J|\sin(q/2)|$, respectively, where J is the strength of the intrachain couplings [43]. To describe the shape of the spinon continuum in $Sr_2V_3O_9$, $J = 7.1(1)$ meV is determined by a χ^2 fit of the spinon continuum and the corresponding boundaries are overplotted in Fig. 2(b) as dashed lines. The value of J we determine agrees well with our and prior values found from magnetic susceptibility measurements, 7.07 meV [19]. Weak scattering intensities are observed outside the continuum boundary, including a steplike excitation below ∼12 meV and a broad flat band around ∼23 meV. Since these features exhibit no systematic wave vector dependence [38], they may be ascribed to the background scattering due to possible oxygen deficiency and the consequent valence variance of the vanadium ions or to multiple scattering involving elastic incoherent scattering from vanadium followed by inelastic scattering from the spinon continuum or aluminum phonons [48] of the sample environment, respectively.

Various analytical and numerical methods have been developed to describe the dynamical structure factor of the HAFMCs. Here we first compare the INS spectra of $Sr_2V_3O_9$ to the cross section calculated by the Bethe ansatz. The 2-spinon continuum is known to account for ∼71% of the total spectral weight [29,46,49,50], while the remaining spectral weight is mostly accounted for by the 4-spinon continuum [29,46,51]. As a zero temperature calculation method, the comparison with the experimental data acquired at 5 K is justified since the overall bandwidth of the system, which sets the relevant energy scale of the 1D fluctuations, is at much higher energy scales than the measuring temperature.

For $J = 7.1$ meV, the calculated spectral function is shown on the right panel in Fig. 2(b). The calculated data are convolved by a Gaussian function with a full width at half maximum of $\Delta Q = 0.1$ r.l.u. along the Q axis and by the instrumental energy resolution along the E axis [38]. More detailed comparisons for scans at constant Q and E are presented in Figs. 2(c) and 2(d), respectively. For the background scan at $h = 0$, the intensity is fitted by a Gaussian function plus a step function to account for the additional scattering at ∼12 meV described earlier. This is then added to the other calculated spectra shown in Figs. 2(c) and 2(d). The calculation reproduces the INS spectra, thus confirming the existence of HAFMCs in $Sr_2V_3O_9$.

The obtained strength of the intrachain coupling of $J = 7.1(1)$ meV, together with the magnetic long-range order transition temperature $T_N = 5.3$ K, allows an estimate of the strength of the ferrromagnetic interchain coupling $J_\perp$. Following the mean field analysis [19,52], $|J_\perp|$ is estimated to be ∼0.16 meV, which is ∼2.3% of the intrachain coupling J. This agrees well with the extent of the dispersion measured orthogonal to the chain direction [38].

In order to resolve a possible gap in the spinon excitations, further INS experiments were performed with lower incident energies of $E_i = 10$ and 4 meV. Figure 3 summarizes the spectra after full integrations along directions perpendicular to the chain. As compared in Figs. 3(b) and 3(d), the spectra at $(1/2, 0, -1/2)$ follows the theoretical dynamical structure factor down to ∼0.1 meV. Therefore, it can be concluded that the spinon excitations in $Sr_2V_3O_9$ are gapless within the instrumental resolution of ∼0.1 meV.

The temperature evolution of the INS spectra is summarized in Fig. 4. For $T = 20$ and 50 K, the constant-E map at an energy transfer of $E = 3$ meV is compared in Fig. 4(a). The main features are similar to the map at $T = 5$ K shown in Fig. 2(a), but the scattering intensity is weaker at elevated temperatures. Figure 4(b) compares the intensity along the $(h, 0, h)$ direction at $T = 5$, 20, and 50 K. The intensity contrast along the streaks is reduced at elevated temperatures as thermal fluctuations overcome the interchain couplings.

After integration in the range of $\delta h = [-1.2, 1.2]$ r.l.u. along the $(h, 0, h)$ direction, the spectral functions along $(h, 0, -h)$ are compared in Fig. 4(c) for $T = 20$ and 50 K. The dashed lines outline the 2-spinon continuum for $J = 7.1$ meV as in Fig. 2(b). Besides the reduced scattering intensities, the excitations become softened at elevated temperatures, with a significant fraction of the scattering intensity lying below $\omega_L(q)$ at $T = 50$ K.

According to theoretical calculations [53], an intensity transfer from $(h = 1/2, \omega \to 0)$ to $(h = 0, \omega \to 0)$ is expected in the spectra function $S(q, \omega)$ at elevated temperatures due to thermal fluctuations. Although such an intensity transfer is not directly probed in our experiment, it may induce a peak at nonzero energies in the constant-Q scan at $h = 0.5$ as the zero energy intensity is greatly reduced. Figure 4(d) compares the constant-Q scans at $h = 0.5$ for $T = 5$, 20, and 50 K. Theoretical spectral functions calculated by the DMRG method at the corresponding temperatures are plotted as red solid lines, which reproduce the spectral function over a large range of energy transfers. At $T = 50$ K, the reduced intensities around $E = 0$ are consistent with the theoretical prediction of the HAFMCs, thus confirming the chain physics in $Sr_2V_3O_9$.

The temperature evolution of the scattering intensity for $S = 1/2$ HAFMCs has also been investigated through effective field theories in the continuum limit [54,55]. At relatively low energy transfers, the energy dependence of the cross section at $\boldsymbol{q} = (1/2, 0, -1/2)$ is expressed as

$$S(\omega) \propto (n_\omega + 1)\mathrm{Im}\left\{\frac{1}{T}\left[\rho\left(\frac{\omega}{4\pi k_B T}\right)\right]^2\right\}, \tag{1}$$

with the $\rho(x)$ function defined as

$$\rho(x) = \frac{\Gamma\left(\frac{1}{4} - ix\right)}{\Gamma\left(\frac{3}{4} - ix\right)}. \tag{2}$$

In this expression, n_ω is the Bose factor and Γ is the complex gamma function. Using this expression, we calculate the cross

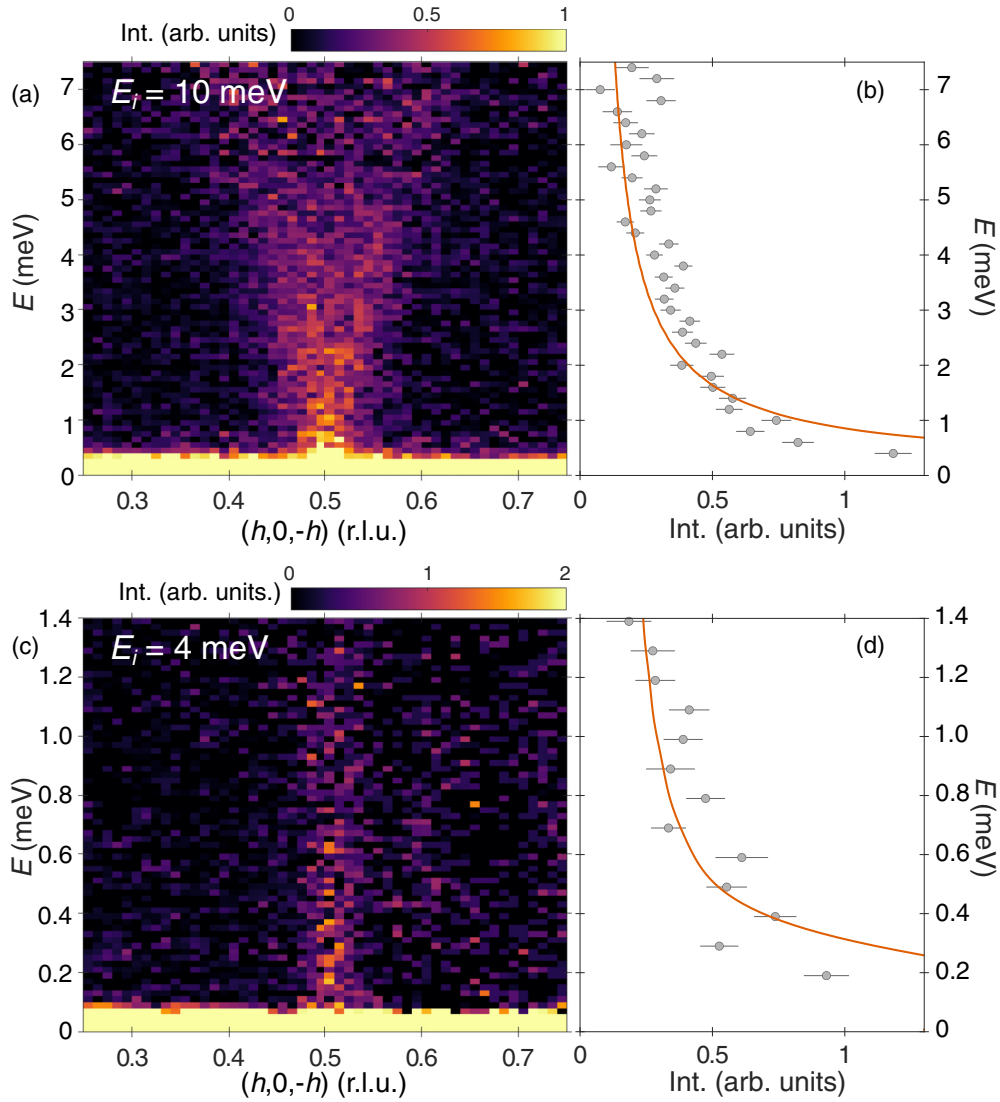

FIG. 3. (a) Low-energy section of the INS spectra $S(Q, \omega)$ measured with an incident neutron energy of $E_i = 10$ meV. Data along directions perpendicular to the chain have been integrated for better statistics. (b) Scattering intensity as a function of E integrated over the range of $\delta h = [0.49, 0.51]$ r.l.u. along $(h, 0, -h)$. The red line is the theoretical scattering cross section for a HAFMC plus a constant background obtained by integration in the range $\delta h = [0.29, 0.31]$ r.l.u. off the spinon continuum. (c),(d) Similar to panels (a),(b) with a lower $E_i = 4$ meV.

section for $S = 1/2$ HAFMCs for energies up to 16 meV. The calculated results, with a fitted scale factor, are shown in Fig. 4(d) as dash-dotted lines. In the calculated energy range, the field theoretical results capture the temperature evolution of both the experimental data and the DMRG results, which further justifies the existence of HAFMCs in $Sr_2V_3O_9$.

Conclusions. The existence of $S = 1/2$ HAFMCs in $Sr_2V_3O_9$ is spectroscopically confirmed through inelastic neutron scattering experiments and comparison with numerical simulations and mean field approximations. A spinon continuum is observed along the $(h, 0, \bar{h})$ direction, verifying that the intrachain couplings are mediated by the nonmagnetic V^{5+} ions and thus confirming the importance of the orbital degree of freedom in determining the chain axis. The spinon continuum, with a bandwidth of ∼22 meV, indicates the strength of the intrachain couplings to be ∼7.1(1) meV. Despite the magnetic transition at $T_N \sim 5.3$ K, the excitations in $Sr_2V_3O_9$ remain gapless down to 5 K. Through comparisons to the Bethe ansatz, the density matrix renormalization group (DMRG) calculations, and the field theories, we conclude that $Sr_2V_3O_9$ is a host of weakly coupled $S = 1/2$ HAFMCs.

Acknowledgments. We acknowledge helpful discussions with Jianda Wu, Jiahao Yang, and Yuan Li. This work was supported by the U.S. Department of Energy, Office of Science, Basic Energy Sciences, Materials Sciences and Engineering Division. This research used resources at the Spallation Neutron Source (SNS) and the High Flux Isotope Reactor (HFIR); both are DOE Office of Science User Facilities operated by the Oak Ridge National Laboratory (ORNL). The beam time was allocated to Proposal No. IPTS-26732.1. The work of S.E.N. and G.A. was supported by the U.S. Department of Energy, Office of Science, National Quantum Information Science Research Centers, Quantum Science Center. Q.C., Q.H., and H.Z. acknowledge support from the National Science Foundation with Grant No. NSF-DMR-2003117.

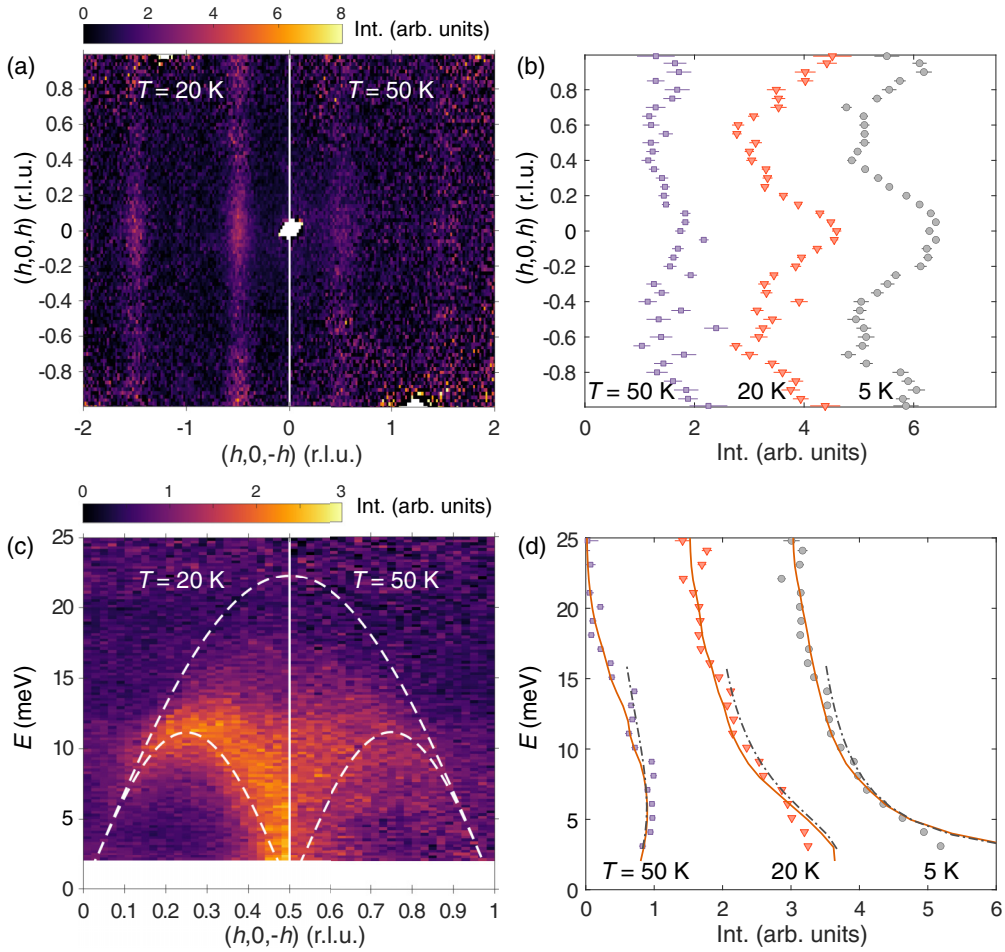

FIG. 4. (a) Constant energy slices of the $Sr_2V_3O_9$ INS spectra $S(Q, \omega)$ in the $(h, 0, l)$ plane measured at $T = 20$ (left) and 50 K (right). Data is integrated over the energy range of [2,4] meV and is plotted on an orthogonal coordinate system for clarity. (b) Comparison of the scattering intensity along $(h, 0, h)$ measured at $T = 5$ (gray circles), 20 (red triangles), and 50 K (purple squares). Data is integrated over the range of $\delta h = [0.45, 0.55]$ r.l.u. along $(h, 0, -h)$ and $E = [2, 4]$ meV. Data at 20 (50) K is shifted along the x axis by 1.5 (3) for clarity. (c) $S(Q, \omega)$ along $(h, 0, -h)$ measured at $T = 20$ (left) and 50 K (right). Data is integrated over the range of $\delta h = [-1.2, 1.2]$ r.l.u. along $(h, 0, h)$ and $\delta k = [-4, 4]$ r.l.u. along $(0, k, 0)$. Dashed lines are the lower and upper boundaries of the 2-spinon continuum for $J = 7.1$ meV. (d) Comparison of the scattering intensity as a function of E measured at $T = 5$ (gray circles), 20 (red triangles), and 50 K (purple squares). Data is integrated over the range of $\delta h = [0.475, 0.525]$ along $(h, 0, -h)$. At each temperature, the spectra at $Q = 0$ measured at $T = 5$ K is subtracted as the background. Red solid (black dash-dotted) lines are theoretical scattering cross sections calculated by DMRG (field theory) at $T = 50$, 20, and 0 K (50, 20, and 5 K) assuming $J = 7.1$ meV. Data at 20 (50) K is shifted along the x axis by 1.5 (3) units for clarity.

[1] T. Giamarchi, *Quantum Physics in One Dimension* (Clarendon Press, Oxford, 2003).

[2] H. Bethe, Zur Theorie der Metalle. I. Eigenwerte und Eigenfunktionen der linearen Atomkette, Z. Phys. **71**, 205 (1931).

[3] L. D. Faddeev and L. A. Takhtajan, What is the spin of a spin wave? Phys. Lett. A **85**, 375 (1981).

[4] I. Affleck, T. Kennedy, E. H. Lieb, and H. Tasaki, Rigorous results on valence-bond ground states in antiferromagnets, Phys. Rev. Lett. **59**, 799 (1987).

[5] B. Sutherland, *Beautiful Models: 70 Years of Exactly Solved Quantum Many-Body Problems* (World Scientific, Singapore, 2004).

[6] H. Shiba, Quantization of magnetic excitation continuum due to interchain coupling in nearly one-dimensional Ising-like antiferromagnets, Prog. Theor. Phys. **64**, 466 (1980).

[7] R. Coldea, D. A. Tennant, E. M. Wheeler, E. Wawrzynska, D. Prabhakaran, M. Telling, K. Habicht, P. Smeibidl, and K. Kiefer, Quantum criticality in an Ising chain: Experimental evidence for emergent E_8 symmetry, Science **327**, 177 (2010).

[8] B. Grenier, S. Petit, V. Simonet, E. Canévet, L.-P. Regnault, S. Raymond, B. Canals, C. Berthier, and P. Lejay, Longitudinal and transverse Zeeman ladders in the Ising-like chain antiferromagnet $BaCo_2V_2O_8$, Phys. Rev. Lett. **114**, 017201 (2015).

[9] M. Mena, N. Hänni, S. Ward, E. Hirtenlechner, R. Bewley, C. Hubig, U. Schollwöck, B. Normand, K. W. Krämer, D. F.

McMorrow, and Ch. Rüegg, Thermal control of spin excitations in the coupled Ising-chain material $RbCoCl_3$, Phys. Rev. Lett. **124**, 257201 (2020).

[10] H. Lane, C. Stock, S.-W. Cheong, F. Demmel, R. A. Ewings, and F. Krüger, Nonlinear soliton confinement in weakly coupled antiferromagnetic spin chains, Phys. Rev. B **102**, 024437 (2020).

[11] M. Karbach and G. Müller, Line-shape predictions via Bethe ansatz for the one-dimensional spin-$\frac{1}{2}$ Heisenberg antiferromagnet in a magnetic field, Phys. Rev. B **62**, 14871 (2000).

[12] M. Karbach, D. Biegel, and G. Müller, Quasiparticles governing the zero-temperature dynamics of the one-dimensional spin-1/2 Heisenberg antiferromagnet in a magnetic field, Phys. Rev. B **66**, 054405 (2002).

[13] Z. Wang, J. Wu, W. Yang, A. K. Bera, D. Kamenskyi, A. T. M. N. Islam, S. Xu, J. M. Law, B. Lake, C. Wu, and A. Loidl, Experimental observation of Bethe strings, Nature (London) **554**, 219 (2018).

[14] W. Yang, J. Wu, S. Xu, Z. Wang, and C. Wu, One-dimensional quantum spin dynamics of Bethe string states, Phys. Rev. B **100**, 184406 (2019).

[15] Z. Wang, M. Schmidt, A. Loidl, J. Wu, H. Zou, W. Yang, C. Dong, Y. Kohama, K. Kindo, D. I. Gorbunov, S. Niesen, O. Breunig, J. Engelmayer, and T. Lorenz, Quantum critical dynamics of a Heisenberg-Ising chain in a longitudinal field: Many-body strings versus fractional excitations, Phys. Rev. Lett. **123**, 067202 (2019).

[16] A. K. Bera, J. Wu, W. Yang, R. Bewley, M. Boehm, J. Xu, M. Bartkowiak, O. Prokhnenko, B. Klemke, A. T. M. N. Islam, J. M. Law, Z. Wang, and B. Lake, Dispersions of many-body Bethe strings, Nat. Phys. **16**, 625 (2020).

[17] J. Yang, X. Wang, and J. Wu, Magnetic excitations in the one-dimensional Heisenberg-Ising model with external fields and their experimental realizations, J. Phys. A: Math. **56**, 013001 (2023).

[18] J. Yang, T. Xie, S. E. Nikitin, J. Wu, and A. Podlesnyak, Confinement of many-body Bethe strings, Phys. Rev. B **108**, L020402 (2023).

[19] E. E. Kaul, H. Rosner, V. Yushankhai, J. Sichelschmidt, R. V. Shpanchenko, and C. Geibel, $Sr_2V_3O_9$ and $Ba_2V_3O_9$: Quasi-one-dimensional spin-systems with an anomalous low temperature susceptibility, Phys. Rev. B **67**, 174417 (2003).

[20] V. A. Ivanshin, V. Yushankhai, J. Sichelschmidt, D. V. Zakharov, E. E. Kaul, and C. Geibel, ESR study of the anisotropic exchange in the quasi-one-dimensional antiferromagnet $Sr_2V_3O_9$, Phys. Rev. B **68**, 064404 (2003).

[21] O. Mentre, A.-C. Dhaussy, F. Abraham, and H. Steinfink, Structural, infrared, and magnetic characterization of the solid solution series $Sr_{2-x}Pb_x(VO)(VO_4)_2$; Evidence of the $Pb^{2+}6s^2$ lone pair stereochemical effect, J. Solid State Chem. **140**, 417 (1998).

[22] M. Uesaka, T. Kawamata, N. Kaneko, M. Sato, K. Kudo, N. Kobayashi, and Y. Koike, Thermal conductivity of the quasi one-dimensional spin system $Sr_2V_3O_9$, J. Phys.: Conf. Ser. **200**, 022068 (2010).

[23] T. Kawamata, M. Uesaka, M. Sato, K. Naruse, K. Kudo, N. Kobayashi, and Y. Koike, Thermal conductivity due to spinons in the one-dimensional quantum spin system $Sr_2V_3O_9$, J. Phys. Soc. Jpn. **83**, 054601 (2014).

[24] H.-J. Koo and M.-H. Whangbo, Spin dimer analysis of the magnetic structures of $A_2V_3O_9$ (A=Ba, Sr) and η-$Na_9V_{14}O_{35}$: Importance of the V^{4+}-O$\cdots$O-V^{4+} super-superexchange interactions mediated by the O-V^{5+}-O bridges, Solid State Sci. **9**, 824 (2007).

[25] A. Rodríguez-Fortea, M. Llunell, P. Alemany, and E. Canadell, First-principles study of the interaction between paramagnetic V^{4+} centers through formally magnetically inactive VO_4 tetrahedra in the quasi-one-dimensional spin systems $Sr_2V_3O_9$ and $Ba_2V_3O_9$, Phys. Rev. B **82**, 134416 (2010).

[26] A. Rodríguez-Fortea, M. Llunell, P. Alemany, and E. Canadell, Factors affecting the magnetic coupling in $Sr_2V_3O_9$ type oxides: As for V substitution in the VO_4 tetrahedra and nature of the cation, Dalton Trans. **42**, 15555 (2013).

[27] O. Arnold, J. C. Bilheux, J. M. Borreguero, A. Buts, S. I. Campbell, L. Chapon, M. Doucet, N. Draper, R. Ferraz Leal, M. A. Gigg, V. E. Lynch, A. Markvardsen, D. J. Mikkelson, R. L. Mikkelson, R. Miller, K. Palmen, P. Parker, G. Passos, T. G. Perring, P. F. Peterson *et al.*, Mantid-data analysis and visualization package for neutron scattering and μ SR experiments, Nucl. Instrum. Methods Phys. Res. A **764**, 156 (2014).

[28] J.-S. Caux, Correlation functions of integrable models: A description of the ABACUS algorithm, J. Math. Phys. **50**, 095214 (2009).

[29] J.-S. Caux and R. Hagemans, The four-spinon dynamical structure factor of the Heisenberg chain, J. Stat. Mech. (2006) P12013.

[30] S. R. White, Density matrix formulation for quantum renormalization groups, Phys. Rev. Lett. **69**, 2863 (1992).

[31] S. R. White, Density-matrix algorithms for quantum renormalization groups, Phys. Rev. B **48**, 10345 (1993).

[32] G. Alvarez, The density matrix renormalization group for strongly correlated electron systems: A generic implementation, Comput. Phys. Commun. **180**, 1572 (2009).

[33] T. D. Kühner and S. R. White, Dynamical correlation functions using the density matrix renormalization group, Phys. Rev. B **60**, 335 (1999).

[34] A. Nocera and G. Alvarez, Spectral functions with the density matrix renormalization group: Krylov-space approach for correction vectors, Phys. Rev. E **94**, 053308 (2016).

[35] A. E. Feiguin and S. R. White, Finite-temperature density matrix renormalization using an enlarged Hilbert space, Phys. Rev. B **72**, 220401(R) (2005).

[36] A. E. Feiguin and G. A. Fiete, Spectral properties of a spin-incoherent Luttinger liquid, Phys. Rev. B **81**, 075108 (2010).

[37] A. Nocera and G. Alvarez, Symmetry-conserving purification of quantum states within the density matrix renormalization group, Phys. Rev. B **93**, 045137 (2016).

[38] See Supplemental Material at http://link.aps.org/supplemental/10.1103/PhysRevB.109.L020402 for discussions on the background scattering and interchain couplings, together with the input files and the calculation details of the DMRG calculations. It includes Ref. [39].

[39] A. Scheie, P. Laurell, A. M. Samarakoon, B. Lake, S. E. Nagler, G. E. Granroth, S. Okamoto, G. Alvarez, and D. A. Tennant, Witnessing entanglement in quantum magnets using neutron scattering, Phys. Rev. B **103**, 224434 (2021).

[40] R. Feyerherm, S. Abens, D. Günther, T. Ishida, M. Meißner, M. Meschke, T. Nogami, and M. Steiner, Magnetic-field induced gap and staggered susceptibility in the S = 1/2

chain $[PM \cdot Cu(NO_3)_2 \cdot (H_2O)_2]_n$ (PM = pyrimidine), J. Phys.: Condens. Matter **12**, 8495 (2000).

[41] D. C. Dender, P. R. Hammar, D. H. Reich, C. Broholm, and G. Aeppli, Direct observation of field-induced incommensurate fluctuations in a one-dimensional $S = 1/2$ antiferromagnet, Phys. Rev. Lett. **79**, 1750 (1997).

[42] M. Oshikawa and I. Affleck, Field-induced gap in $S = 1/2$ antiferromagnetic chains, Phys. Rev. Lett. **79**, 2883 (1997).

[43] G. Müller, H. Thomas, H. Beck, and J. C. Bonner, Quantum spin dynamics of the antiferromagnetic linear chain in zero and nonzero magnetic field, Phys. Rev. B **24**, 1429 (1981).

[44] D. A. Tennant, R. A. Cowley, S. E. Nagler, and A. M. Tsvelik, Measurement of the spin-excitation continuum in one-dimensional $KCuF_3$ using neutron scattering, Phys. Rev. B **52**, 13368 (1995).

[45] B. Lake, D. A. Tennant, C. D. Frost, and S. E. Nagler, Quantum criticality and universal scaling of a quantum antiferromagnet, Nat. Mater. **4**, 329 (2005).

[46] M. Mourigal, M. Enderle, A. Klöpperpieper, J.-S. Caux, A. Stunault, and H. M. Rønnow, Fractional spinon excitations in the quantum Heisenberg antiferromagnetic chain, Nat. Phys. **9**, 435 (2013).

[47] L. S. Wu, S. E. Nikitin, Z. Wang, W. Zhu, C. D. Batista, A. M. Tsvelik, A. M. Samarakoon, D. A. Tennant, M. Brando, L. Vasylechko, M. Frontzek, A. T. Savici, G. Sala, G. Ehlers, A. D. Christianson, M. D. Lumsden, and A. Podlesnyak, Tomonaga-Luttinger liquid behavior and spinon confinement in $YbAlO_3$, Nat. Commun. **10**, 698 (2019).

[48] M. Kresch, M. Lucas, O. Delaire, J. Y. Y. Lin, and B. Fultz, Phonons in aluminum at high temperatures studied by inelastic neutron scattering, Phys. Rev. B **77**, 024301 (2008).

[49] A. H. Bougourzi, M. Couture, and M. Kacir, Exact two-spinon dynamical correlation function of the one-dimensional Heisenberg model, Phys. Rev. B **54**, R12669(R) (1996).

[50] M. Karbach, G. Müller, A. H. Bougourzi, A. Fledderjohann, and K.-H. Mütter, Two-spinon dynamic structure factor of the one-dimensional $S = \frac{1}{2}$ Heisenberg antiferromagnet, Phys. Rev. B **55**, 12510 (1997).

[51] B. Lake, D. A. Tennant, J.-S. Caux, T. Barthel, U. Schollwöck, S. E. Nagler, and C. D. Frost, Multispinon continua at zero and finite temperature in a near-ideal Heisenberg chain, Phys. Rev. Lett. **111**, 137205 (2013).

[52] H. J. Schulz, Dynamics of coupled quantum spin chains, Phys. Rev. Lett. **77**, 2790 (1996).

[53] O. A. Starykh, A. W. Sandvik, and R. R. P. Singh, Dynamics of the spin-$\frac{1}{2}$ Heisenberg chain at intermediate temperatures, Phys. Rev. B **55**, 14953 (1997).

[54] H. J. Schulz, Phase diagrams and correlation exponents for quantum spin chains of arbitrary spin quantum number, Phys. Rev. B **34**, 6372 (1986).

[55] D. A. Tennant, T. G. Perring, R. A. Cowley, and S. E. Nagler, Unbound spinons in the S = 1/2 antiferromagnetic chain $KCuF_3$, Phys. Rev. Lett. **70**, 4003 (1993).